Dynamic modeling of aerostatic bearing spindle and measurement of surface topographies in ultra-precision raster milling

S. To[1,#], S.J. Zhang[1], H.T. Wang[1], S.J. Wang[1]

1 State Key Laboratory in Ultra-precision Machining Technology, Department of Industrial and Systems Engineering, The Hong Kong Polytechnic University, Hung Hom, Kowloon, Hong Kong SAR, China.

Corresponding Author / E-mail: mfsto@inet.polyu.edu.hk, TEL: +852-2766-6587, FAX: +852-2764-7657

KEYWORDS : Spindle Vibration, Surface Generation, Dynamic Modeling, Aerostatic Bearing Spindle, Ultra-precision Raster Milling

In ultra-precision raster milling (UPRM), surface topography is determined by multi-factors. In this paper, spindle vibration and its impact on surface topography is investigated. A dynamic model of an aerostatic bearing spindle under the excitation of intermittent cutting forces in UPRM is proposed to explore its vibration, involving translational motions at the frequencies of 560Hz in the radial direction and of 470Hz in the spin axial direction and a tilting motion at the frequency of 1230Hz. The simulation of surface generation is developed to exhibit that the spindle vibration produces aliased patterns on a surface topography, where the aliased patterns are generated as a result of uniform phase shifts of the spindle vibration for each profile in the feed direction and eliminated because of random phase shifts. The Optical Profiling System (WYKO NT8000) is utilized to measure surface topographies of machined specimens to identify the characteristic topographies. Experimental and theoretical results produce a great agreement. The dynamic model is proposed to explain the spindle vibration which also takes an important impact on surface topography in UPRM.

Manuscript received: January XX, 2011 / Accepted: January XX, 2011

NOMENCLATURE

m = spindle rotor mass
k= stiffness of a pressure air
e= eccentric position of the mass
l=position of the centre of mass center relative to its equilibrium along the z-axis
R =Radius of spindle rotor
J=inertial tensor
d_2=distance of tilting center of spin rotor to the tool
μ=damper ratio
ω= spindle speed
f_r = feed rate
d_o = depth of cut
d_1= swing distance
R_r = tool nose radius
θ and Φ= tilting angles of the spin rotor
$O(XYZ)$= inertial coordinate system
$o(xyz)$= reference system
ω=spindle speed
t=machining time
$\Omega = \omega t$
F_r=raster cutting force
F_t=thrust cutting force
F_m=main cutting force
f=frequency of spindle rotor
a= amplitude of one corresponding frequency
φ=phase angle of one corresponding frequency

1. Introduction

Ultra-precision raster milling (UPRM) is an ultra-precision machining technique for fabricating non-rotational freeform surfaces with nanometric surface roughness and sub-micrometric form accuracy without the need for any subsequent polishing. Surface topography or surface roughness plays an extremely important role in estimating components' surface quality. In UPRM, some researchers have focused on studying the influence of multi-factors on surface topographies. Cheung et al. [1] presented a framework of a model-based simulation system for the prediction of the surface generation in ultra-precision multi-axis raster milling of freeform surfaces. In 2006, he and his partners [2] developed a model-based simulation system for prediction of form accuracy in UPRM of optical freeform surfaces, which majorly took into account the cutting mechanics, cutting strategies and the kinematics of the cutting process. Cheng et al. [3~5] proposed a theoretical model to predict surface roughness and utilized the model to optimize cutting conditions (tool tip geometry, spindle speed, depth of cut, feed rate, swing distance, and step distance) and cutting strategies (horizontal cutting and vertical cutting) in UPRM. Kong et al. [6] employed a theoretical dynamics model in UPRM for surface generation, and in 2009 he and his co-authors [7] discussed the factors influencing surface generation in UPRM, which results show that cutting conditions, tool geometry, cutting strategies and tool wear takes a major impact on surface roughness, and cutting strategies, tool path generation and kinematic errors of sliders principally influences the form accuracy of freeform surfaces.

Also, some researchers have discussed influence of spindle vibration on surface profiles. Martin et al. [8] examined and discussed those spindle errors, surface finish and form errors of machined parts, which result indicates the spindle vibration influences surface topographies of machined parts. Marsh [9] discussed the effects of spindle dynamics on topographies of the flat surfaces in precision fly-cutting. An et al. [10] experimentally and theoretically identified that the tilting motions of aerostatic bearing spindle influences topographies of machined surfaces in ultra-precision fly cutting. However, little attention has been paid to an impact of aerostatic bearing spindle vibration excited by intermittent cutting forces and mass eccentricity of its spin rotor in the axial direction, in the radial direction in the rotational direction on surface topography in UPRM.

So in this paper, dynamic behaviours of an areostatic bearing spindle in UPRM with translational motions in the radial and axial direction and with a tilting motion around the radial direction and its impact on surface topography are theoretically and experimentally discussed. Firstly, the aerostatic bearing spindle system is idealized and simplified as a spring-mass-damper system excited by periodical intermittent cutting forces to explore the spindle dynamic characteristics by building dynamic equations. Secondly, a simulated topographical surface generation model is developed to produce surface topographies so as to estimate the impact of the aerostatic bearing spindle vibration. Finally, to identify the previous theoretical results, machined surface topographies are measured by the Optical Profiling System (WYKO NT8000).

2. Experimental setups

2.1 UPRM mechanism and spindle performance specifications

All flat-cutting tests were performed on an UPRM machine (Precitech Freeform 705G, Precision Inc., USA) as shown in Fig.1. The UPRM machine system possesses three linear axes (X, Y and Z) and two rotational axes (B and C), a diamond tool is rotated with the spindle being set up on the C axis to intermittently cut a work-piece and the work-piece is installed on the B axis rotation table. The surface roughness profile for the machined surface is formed by the repetition of the tool tip profile at intervals of the tool feed rate along the feed direction and then intervals of a step distance along the raster direction under cutting conditions by two cutting strategies, e.g. horizontal cutting that the feed direction is horizontal in the X-axial direction and vertical cutting that the feed direction is vertical in the Y-axial direction.

The spindle rotating around the spin axis is flowed and supported by a constant pressure air film, so the intermittent cutting forces and its self-eccentricity mass will induce the spindle vibration. The spindle performance specifications of the UPRM machine are tabulated in Tab.1. The experimental tests were carried out on the UPRM machine to flat-mill copper alloys under cutting conditions of Tab.2 by horizontal cutting to validate the impact of the spindle vibration on surface topography.

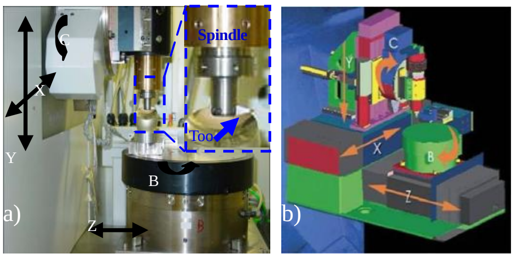

Fig.1 An UPRM machine a) Precitech Freeform 705G and b) its schematic configuration

Tab.1 Spindle performance specifications

Spindle rotor mass (m) (kg)	0.5+2
Radial stiffness (k_2/ k_3) (N/μm)	22
Axial stiffness (k_1) (N/μm)	31
Eccentric position of the mass imbalance away from the rotor axis (e) (μm)	0.5
Position of the centre of mass center relative to its equilibrium along the z-axis (l_1/ l_2) (mm)	100+2e / 100-2e
Radius of spindle rotor (R) (mm)	25
Inertial tensor around y-axis (J_y) (gm^2)	0.25
Inertial tensor around z/x-axis (J_z/J_x) (gm^2)	4
The distance of tilting center of spin rotor to the tool (d_2) (mm)	180
Damper ratio μ	0.05

Tab.2 Cutting conditions

Spindle speed (ω) (rpm)	4000
Feed rate (f_r) (mm/min)	60
Depth of cut (d_o) (μm)	3
Swing distance (d_1) (mm)	23
Step distance (s_r) (μm)	10
Tool nose radius (R_r) (mm)	0.78
Tool rake angle (°)	0
Front clearance angle (°)	15
Cutting strategy	Horizontal cutting

2.2 Measurement of surface topographies

The Optical Profiling System (WYKO NT8000) was utilized to measure surface topographies of machined specimens to estimate effects of the aerostatic bearing spindle vibration on surface topography. Surface topography data were acquired under an effective magnification 10X within an effective field of view of 0.636mmx0.477mm.

2.3 Measurement of cutting forces

To measure intermittent cutting forces, a Kistler 9252A force transducer was mounted between a work-piece and a fixture positioned on the B-axis with a pre-loading force to sense cutting forces. The signals of the cutting forces in the three directions were recorded by a NI PCI-6132 14 bits multifunction DAQ card at the sampling frequency 1MHz after being pre-amplified by a charge amplifier.

3. Modeling of aerostatic bearing spindle and simulation of surface generation

3.1 Modeling of spin rotor motions

To simulate dynamic response of the aerostatic bearing spindle in UPRM, involving the radial, axial and tilting motions (shown in Fig.3), the spindle system is simply idealized as a multi-spring-mass-damper system. And, the spin rotor approximated by a single point mass is seen as a rigid body supported by an air film represented by a series of springs in the axial and radial directions. The spring stiffness distribution along the journal length is also considered as a constant value. Its schematic diagram is shown in Fig.4. The spin rotor is replaced by *m*, *x*, *y* and *z* express translational displacements of its spin rotor, *c* represents viscous dampers and *k* denotes stiffness of springs, *e* represents an eccentric distance, and θ and Φ mean tilting angles of the spin rotor around the radial axis, respectively.

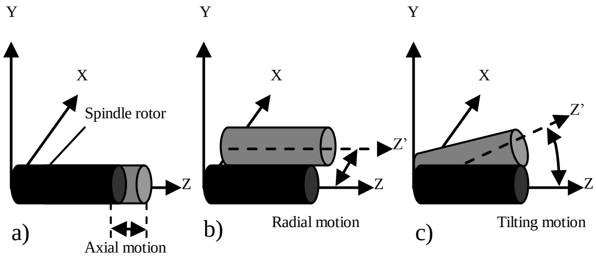

Fig.3 Schematic diagrams of spin rotor motions a) axial motion, b) radial motion and c) tilting motion

The dynamic formula is described by Euler equations of motion, which includes three translational motions and three rotational motions in a three-dimensional space. Fig.5 shows that the spin rotor is referred to a reference system *o*(*xyz*) moving in an inertial coordinate system *O*(*XYZ*) with the rotor's eccentricity mass *m*. So its motions can be described by the rotations of the inertial coordinate system *O*(*XYZ*) around the *z*, *x* and *y*-axis with the angles (θ, Φ and Ω) of the reference coordinate system *o*(*xyz*) as shown in Fig.5a and by the translations of the inertial coordinate system *O*(*XYZ*) along the *x*, *y* and *z*-axis with the displacements (*x*, *y* and *z*, respectively) of the reference coordinate system *o*(*xyz*) as shown in Fig.5b, as below:

1) Translation along the *x*-axis, x_o;
2) Translation along the *y*-axis, y_o;
3) Translation along the *z*-axis, z_o;
4) Rotation around the *Z*-axis, θ;
5) Rotation around the X_1-axis, ϕ;
6) And rotation around the *y*-axis, Ω.

where, Ω is equal to ωt, in which ω is the spindle speed and *t* is time.

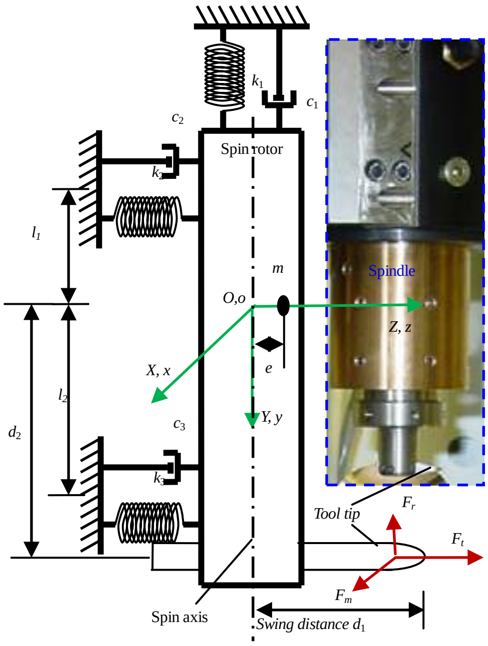

Fig.4 Schematic diagram of an aerostatic bearing spindle

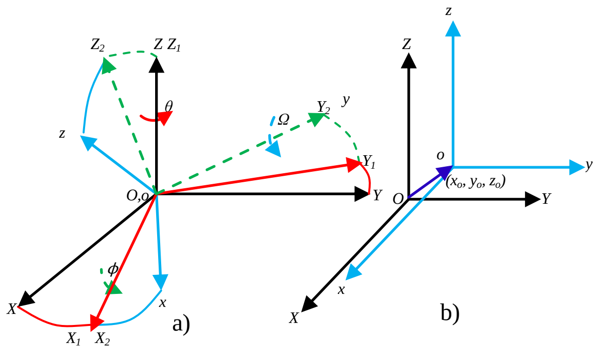

Fig.5 The coordinate transforms a) translational transform and b) rotational transform

The mass center coordinate $\vec{e}$ in *o*(*xyz*) is expressed as:

$$\vec{e}=\begin{bmatrix} e_x \\ e_y \\ e_z \end{bmatrix}=\begin{bmatrix} 0 \\ 0 \\ e \end{bmatrix}. \tag{1}$$

And, since the spin rotor is symmetric, the inertial tensor in *o*(*xyz*) is displayed as:

$$\begin{aligned} J &= \begin{bmatrix} J_x & -J_{xy} & -J_{xz} \\ -J_{yx} & J_y & -J_{yz} \\ -J_{zx} & -J_{zy} & J_z \end{bmatrix} \\ &= \begin{bmatrix} J_x & -me(l_1-l_2) & 0 \\ -me(l_1-l_2) & J_y & -me(l_1-l_2) \\ 0 & -me(l_1-l_2) & J_z \end{bmatrix} \end{aligned}. \tag{2}$$

Based on Newton's Laws and Theorem of Angular Momentum [11], the corresponding equations of the spindle rotor motions are:

$$\begin{cases} m\ddot{y}+k_1y=me(\omega^2\sin\sqrt{\theta^2+\phi^2}+\dot{\phi}^2\cos\phi+\dot{\theta}^2\cos\theta)+\{-F_r\} \\ m\ddot{x}+k_2x=me(\omega^2+\dot{\phi}^2\sin\phi)\sin\omega t+\{-F_m\} \\ m\ddot{z}+k_3z=me(\omega^2+\dot{\theta}^2\sin\theta)\cos\omega t+\{-F_t\} \\ J_x\ddot{\phi}+(J_x-J_y)\omega\dot{\theta}=-(k_2+k_3)(l_1{}^2+l_2{}^2)\phi \\ \quad -k_1R^2\phi+me\omega^2(l_1-l_2)+\{+F_rd_1-F_td_2\} \\ J_z\ddot{\theta}-(J_z-J_y)\omega\dot{\phi}=-(k_2+k_3)(l_1{}^2+l_2{}^2)\theta-k_1R^2\theta+\{+F_md_2\} \end{cases} \tag{3}$$

where *R* is radius of the spin rotor, $-(k_2+k_3)(l_1{}^2+l_2{}^2)\theta-k_1R^2\theta$ and $-(k_2+k_3)(l_1{}^2+l_2{}^2)\phi-k_1R^2\phi$ are represented as rotational torques of air film around the *x*-axial direction and the *z*-axial direction, respectively, $me\omega^2(l_1-l_2)$ is inertia torque of spin rotor, and F_r is intermittent raster cutting force in the y-axial direction, F_t is intermittent thrust cutting force in the z-axial direction and F_m is intermittent main cutting force in the x-axial direction, which frequency is one per one spindle revolution and the contact time is about arcos$((d_1\text{-}d_o)/d_1)/\pi/\omega*60$. As the damping ratio of the pressure air film is further tiny, the resistance and the drag torques can be negligible.

The numerical solution of these equations was done with a Matlab Simulink model, using the Runge-Kutta method.

3.2 Topographical generation

In the face raster milling process, surface topography in horizontal cutting can be separated into two parts, one is a trajectory of a tool arc center rotating around the spindle axis at the swing distance d_1 in the x-axial direction (or in the feed direction) and the other is surface profile determined by a tool arc in the axial direction y-axis (or in the raster direction). In Fig.4a, the trajectory $A(x(t), y(t), z(t))$ of the tool arc center is described in the raster milling system as:

$$\begin{cases} x(t)= & f_r t + d_1\sin(2\pi\frac{\omega}{60}t+\varphi_0)\cos(\theta+\theta_0)+d_2\sin(\theta+\theta_0) \\ & +a_2\sin(2\pi f_2 t+\varphi_2)+a_3\sin(2\pi f_3 t+\varphi_3) \\ & a_1\sin(2\pi f_1 t+\varphi_1)+d_2(1-\cos(\theta+\theta_0)) \\ y(t)= & +d_2(1-\cos(\phi+\phi_0))+d_1\cos(2\pi\frac{\omega}{60}t+\varphi_0)\sin(\theta+\theta_0) \\ & +d_1\sin(2\pi\frac{\omega}{60}t+\varphi_0)\sin(\phi+\phi_0) \\ z(t)= & d_1\cos(2\pi\frac{\omega}{60}t+\varphi_0)\cos(\phi+\phi_0)+d_2\sin(\phi+\phi_0) \\ & +a_1\cos(2\pi f_2 t+\varphi_2)+a_3\cos(2\pi f_3 t+\varphi_3) \end{cases}, \quad (4)$$

where ω is the spindle speed, f_r is the feed rate of the tool and t is machining time, f_1, f_2 and f_3 are frequencies of spindle rotor in the y-axial direction, the x-axial direction and in the z-axial direction, respectively, a_1, a_2 and a_3 are amplitudes of corresponding frequencies, respectively, and φ_1, φ_2 and φ_3 are phase angles corresponding to these frequencies. In Fig.6b, the surface profile between two adjacent points A_3 and A_4 of the spiral trajectory, which is determined by the tool arc profile in the raster direction can be expressed as:

$$z_3+(1-R_r\cdot\cos(\alpha_2)) \quad \text{and} \quad z_4+(1-R_r\cdot\cos(\beta_2)) \quad (5)$$

$$\alpha_2=0\sim\frac{\pi}{2}+\arctan(\frac{z_4-z_3}{s_r+y_4-y_3})-\arccos\frac{\sqrt{f_r^{\,2}+(z_4-z_3)^2}}{2R_r} \quad (6)$$

$$\beta_2=0\sim\frac{\pi}{2}-\arctan(\frac{z_4-z_3}{s_r+y_4-y_3})-\arccos\frac{\sqrt{f_r^{\,2}+(z_4-z_3)^2}}{2R_r}\,. \quad (7)$$

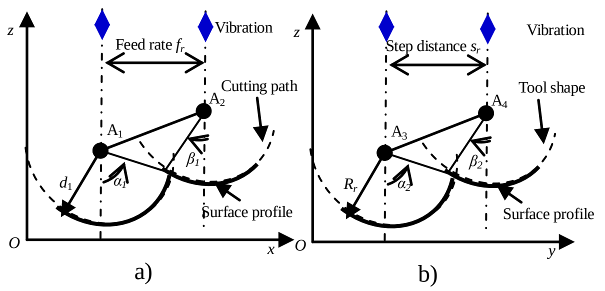

Fig.6 Schematic diagram of surface generation in horizontal cutting a) a horizontal surface profile and b) a vertical surface profile

So, based on the previous model of dynamic response of the aerostatic bearing spindle, x, y, z, θ and ϕ are expressed as the input of the surface generation model, which influence the tool tip trajectory in UPRM. The whole simulation system is shown in Fig.7.

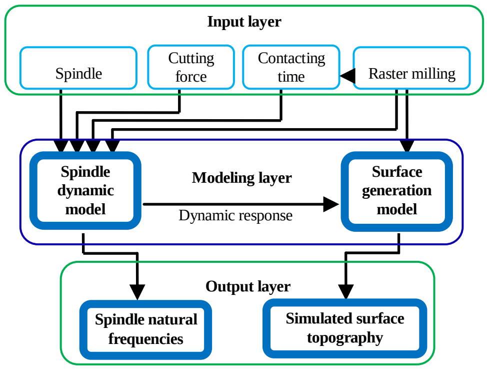

Fig.7 The whole modeling system

4. Results and discussion

4.1 Characteristics of spindle rotor motions

Tab.3 Cutting forces

Main cutting force F_m (N)	0.05
Raster cutting force F_r (N)	0.003
Thrust cutting force F_t (N)	0.05

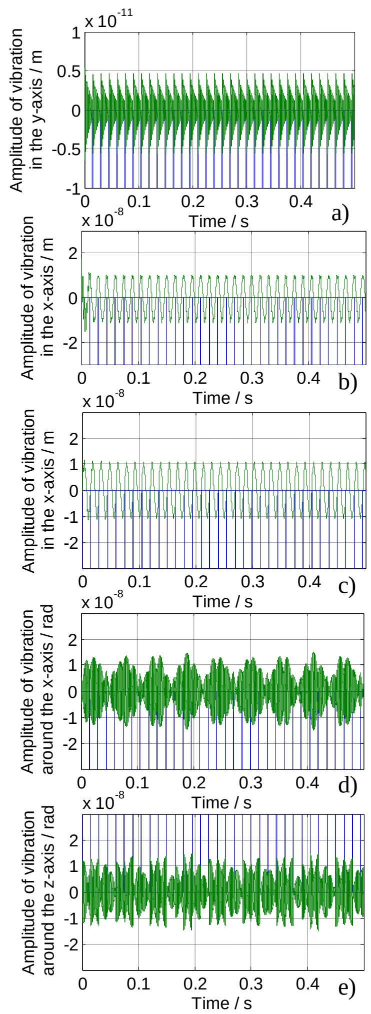

Fig.8 Dynamic response of the spindle motions under interval cutting forces

The Equ.3 is utilized to describe dynamic equations of the spin rotor, where intermittent cutting forces were measured by the Kistler 9252A force transducer and tabulated in Tab.3. To solve these equations by using the Matlab Simulink, the dynamic characteristics of the aerostatic bearing spindle is obtained as shown in Fig.8.

Fig.8a shows that the axial motion of the aerostatic bearing spindle in the *y*-axial direction is almost zero, Fig.8b and c demonstrate the radial motions of the spindle in the *z*-axial direction and in the *x*-axial direction that the spin rotor excited by the intermittent thrust cutting force vibrates in the radial axes and Fig.8d and e present the tilting motions around the *x*-axial direction and the *z*-axial direction. These corresponding frequencies are listed in Tab.4.

Tab.4 Frequencies of the spindle rotor

Tilting frequency around the radial direction (f_1) (Hz)	1231.2
Translational frequency in the spin axial direction (f_2) (Hz)	472.1
Translational frequency in the radial direction (f_3) (Hz)	560.4
Spindle speed (f_4) (Hz)	4000/60

In Fig.8, So the maximal amplitudes a_θ / a_ϕ in the *x*/*z*-axis only induced by the tilting motion around the *z*/*x*-axis are calculated with Equ.8 and 9.

$$a_\theta = d_2 \sin\theta + d_1 \cos\theta - d_1 \quad (8)$$

$$a_\phi = d_2 \sin\phi + d_1 \cos\phi - d_1 \quad (9)$$

And the maximal amplitudes a_θ / a_ϕ in the *y*-axis only induced by the tilting motion around the *z*/*x*-axis are calculated with Equ.10 and 11.

$$a_\phi = d_2 - d_2 \cos\phi + d_1 \sin\phi \quad (10)$$

$$a_\phi = d_2 - d_2 \cos\theta + d_1 \sin\theta \quad (11)$$

So, all amplitudes *as* of the corresponding frequencies are obtained from Fig.8.

4.2 Topographical surface characterization

To estimate surface topographies of milled specimens of copper alloys under cutting conditions of Tab.1 by horizontal cutting, the Optical Profiling System (WYKO NT8000) was employed to measure. Surface topography data were acquired, which patterns show the vibration effect on surface topographies in Fig.9.

In Fig.9a, patterns pointed by arrows periodically occur in the raster direction, which indicates that these patterns were generated by the repetition of the profiles at intervals of tool paths in the feed direction, and the profiles were produced by the repetition of the tool rotation at intervals of feed rate as combining the spindle vibration. So, it is inferred that the phenomenon is induced by vibration.

In Fig.9b, periodical patterns disappear, which is because that the phase shift for each profile induced by spindle vibration is random, and in Fig.9a), the patterns shows that the phase shift for each profile is uniform. According to previous equations of surface generation, the surface topographies are simulated and built up as shown in Fig.10. Fig.10a shows the simulated topography generated with the same phase shift for each profile and Fig.10b indicates the simulated topography produced with the random phase shift for each profile, which theoretically explains the phenomenon in the previous experimental results, corresponding to Fig.9a and b, respectively.

Overall, there is a good agreement between the experimental findings and the simulation results to further support impacts of spindle vibration on topographical surface patterns.

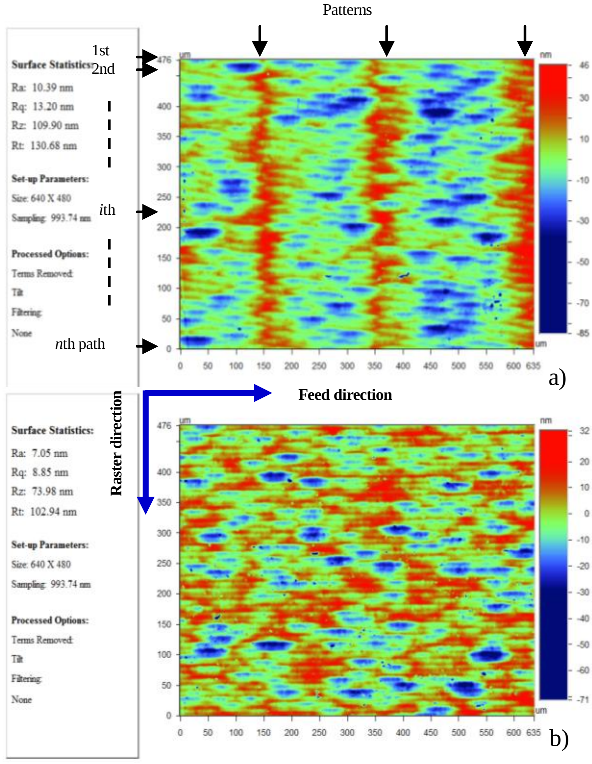

Fig.9 Measured surface topographies by horizontal cutting a) with uniform patterns and b) with random patterns

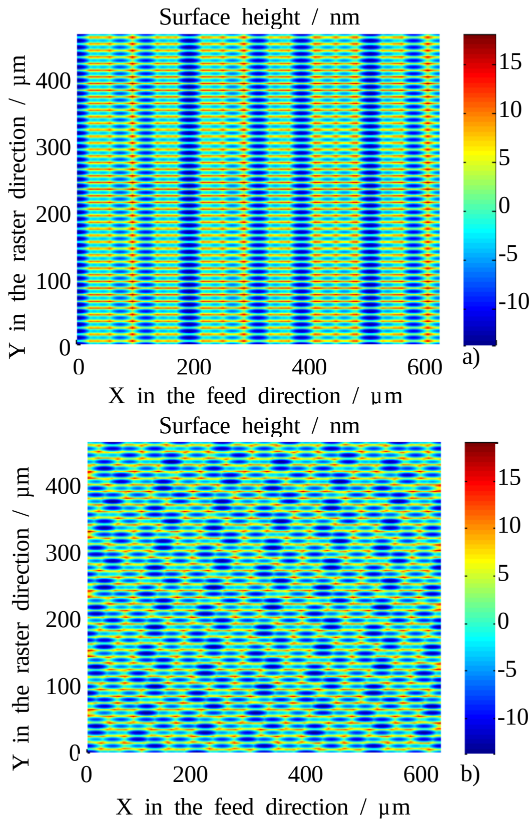

Fig.10 Simulated topographies by horizontal cutting a) under the uniform phase shift and b) under the random phase shift

5. Conclusions

This paper aim is theoretically and experimentally to explore the spindle-induced vibration and its impact on surface topography in UPRM. A dynamic model is proposed to simulate dynamic response of an aerostatic bearing spindle excited by periodic intermittent cutting forces in UPRM to obtain its natural frequencies for translational and tilting motions. A machined surface was examined to identify surface patterns as compared with a simulated surface generation to ascertain the impact of the aerostatic bearing spindle vibration. Some results are as follows:

1) The dynamic model is conducted to simulate dynamic characteristics of the aerostatic bearing spindle in UPRM with its natural frequencies of 472Hz for the translational motion in the axial direction, of 560Hz for the translational motion in the radial direction, of 1231Hz for the tilting motion, respectively.
2) The simulated surface topography generation with the input of the characteristics of the aerostatic bearing spindle vibration is built up to explore that the spindle vibration induces aliased surface patterns formulated by the uniform phase shift and eliminated by the random phase shift.
3) The measured surface topographies of machined specimens identify the characteristic topographies possessing the aliased surface patterns. Experimental and theoretical results produce a great agreement. So, the spindle vibration also intermittently produces modulations on surface topography in UPRM.

ACKNOWLEDGEMENT

The authors express their gratitude to The Research Grants Council of the Hong Kong Special Administrative Region of the People’s Republic of China for providing financial support (Project No. PolyU 5291/08E) and express their sincere thanks to all members of the State Key Laboratory in Ultra-precision Machining Technology in The Hong Kong Polytechnic University for their assistance in the experimental work.

REFERENCES

1. C.F. Cheung, W.B. Lee and S. To, "A framework of a model-based simulation system for predicting surface generation in ultra-precision raster milling of freeform surfaces", Annual of American Society for Precision Engineering Proceedings, Orlando, Florida, Oct.24-19, 2004.
2. C.F. Cheung, L.B. Kong, W.B. Lee and S. To, "Modelling and simulation of freeform surface generation in ultra-precision raster milling", Proc. IMechE Part B: J. Engineering Manufacture, Vol.220, pp.1787-1801, 2006.
3. M.N. Cheng, C.F. Cheung, W.B. Lee and S. To, "Optimization of surface finish in ultra-precision raster milling", Proceedings of Internatinal conference on Leading Edge Manufacturing in 21st century: LEM21 2005(3), pp.1019-1024, 2005.
4. M.N. Cheng, C.F. Cheung, W.B. Lee and S. To, "A study of factors affecting surface quality in ultra-precision raster milling", Key Engineering Materials, Vol.339, pp.400-406, 2007.
5. M.N. Cheng, C.F. Cheung, W.B. Lee, S. To and L.B. Kong, "Theoretical and experimental analysis of nano-surface generation in ultra-precision raster milling", International Journal of Machine Tools and Manufacture, Vol.48, pp.1090-1102, 2008.
6. L.B. Kong, C.F. Cheung, S. To and W.B. Lee, "Development of a dynamic model for ultra-precision raster milling", Key Engineering Materials, Vols.364-366, pp.58-63, 2008.
7. L.B. Kong, C.F. Cheung, S. To and W.B. Lee, "An investigation into surface generation in ultra-precision raster milling", Journal of Materials Processing Technology, Vol.209, pp.4178-4185, 2009.
8. D.L. Martin, A.N. Tabenkin and F.G. Parsons, "Precision spindle and bearing error analysis", Int. J. Mach. Tools Manufact., Vol.35, pp.187-193, 1995.
9. E.R. Marsh, D.A. Arneson, M.J. Van Doren and S.A. Blystone, "The effects of spindle dynamics on precision flycutting", Proceedings of the American society for precision engineering 2005 annual meeting, 2005.
10. C.H. An, Y. Zhang, Q. Xu, F.H. Zhang, J.F. Zhang, L.J. Zhang and J.H. Wang, "Modeling of dynamic characteristic of the aerostatic bearing spindle in an ultra-precision fly cutting machine", International Journal of Machine Tools and Manufacture, Vol.50, pp.374-385, 2010.
11. L. Meirovitch, Methods of analytical dynamics, McGraw-Hill, 1970.